



# Continuum damage modeling of dynamic crack velocity, branching, and energy dissipation in brittle materials

Taufiq Abdullah · Kedar Kirane

Received: 22 September 2020 / Accepted: 7 April 2021 / Published online: 21 April 2021  
© The Author(s), under exclusive licence to Springer Nature B.V. 2021

**Abstract** This study is aimed at evaluating continuum scale predictions of dynamic crack propagation and branching in brittle materials using local damage modeling. Classical experimental results on crack branching in PMMA and the corresponding nonlocal modeling results by Wolff et al. (Int J Numer Meth Eng 101(12):933, 2015) are used as a benchmark. An isotropic damage model based on a frame-invariant effective strain is adapted. Mesh objectivity is achieved by calibrating the damage model for a suitable element size and subsequently retaining that mesh size in all subsequent analyses. Crack propagation and branching are predicted by simulating accurately the test conditions. It is found that a local, rate-independent damage model considerably overpredicts the dynamic crack velocity and the extent of crack branching. Subsequently, the effect of various strain rate-dependent phenomena, viz. material viscoelasticity, rate-dependent strength, fracture energy, and failure strain is evaluated. Incorporating the material strain rate effects is found to improve the predictions and match the test data. In this regard, radially scaling the damage law is found to work the best. Despite an overprediction of micro-branching, the macro-crack branching is found to occur in agreement with the Yoffe instability criterion. Overall, vari-

ous experimentally observed aspects of dynamic cracks are reproduced, including acceleration of cracks to a steady state velocity, increased micro-branching and macro-branching with increased strain rates, and crack velocity dependence of energy dissipation and fracture surface area.

**Keywords** Dynamic fracture · Crack branching · Strain rate dependence · Rate effects · Crack velocity

## 1 Introduction

In many engineering applications involving impact/blast protection and crashworthiness, the energy dissipated by dynamic fracturing is an indicator of performance i.e. a design criterion. However, physical testing is expensive and sometimes infeasible, and designs have to rely on numerical predictions of the same. So, for accurate prediction of energy dissipation, it is crucial for numerical models to correctly predict essential features of dynamic fracture. These include crack velocity and its evolution, crack branching patterns, and the overall extent and geometry of fracturing.

Numerical modeling of dynamic fracture has been pursued via

1. Discrete or line crack representations such as the cohesive crack model (Camacho and Ortiz 1996; Repetto et al. 2000; Barenblatt 1962; Dugdale 1960; Xu and Needleman 1994; Zhou et al. 2005)

T. Abdullah · K. Kirane (✉)  
Department of Mechanical Engineering, Stony Brook  
University, Stony Brook, NY 11794, USA  
e-mail: kedar.kirane@stonybrook.edu

T. Abdullah  
e-mail: taufiq.abdullah@stonybrook.edu

and extended finite element method or XFEM (Xu et al. 2014)

2. Smeared or crack band representations based on continuum damage mechanics (CDM) or the phase-field model (Doan et al. 2017)

The cohesive crack model simulates the fracture process by defining a traction-separation law across the fracture surface. The cohesive traction is a function of the separation such that the fracture energy of the material equals the area under the traction-separation curve. The cohesive crack model is capable of describing crack nucleation, propagation as well as branching. However, the main limitation is the required pre-specification of cohesive elements or interactions along the fracture path which needs to be known beforehand. Hence, when crack branching is expected, FEA models must be built with cohesive elements along all possible crack paths, which can be quite cumbersome. Advanced techniques that allow the addition of cohesive elements on the fly exist too (i.e. dynamic insertion) (Molinari et al. 2007; Pandolfi et al. 1999; Pandolfi and Ortiz 2002). In these methods as the dynamic analysis progresses, cohesive elements are inserted at locations where the stress exceeds a critical value. Various methods for such dynamic insertion of cohesive elements have been discussed by Papoulia et al. (2003). However, these capabilities do not yet exist in most commercially available finite element programs.

The extended finite element method or XFEM was developed by Zi et al. (2005) to overcome this limitation. The method has become widely popular to predict fracture propagation since it yields a mesh independent solution with little to no remeshing. However, crack branching prediction is not automatic and must be achieved by a branching criterion (Jirásek and Rolshoven 2003). Moreover, (Yazid et al. 2009) showed that the XFEM needs a variable number of degrees of freedom per node when it is incorporated into an existing FEM code. It thus takes more processing time to reach a solution. Also, recently both these line crack approaches have been shown to not account properly for damage in the presence of stress triaxiality (Nguyen et al. 2020).

Phase field modeling (PFM) of fracture has become popular in recent years (Li et al. 2016; Bleyer et al. 2017; Nguyen and Wu 2018). Bleyer et al. (2017) demonstrated the application of PFM to dynamic fracture. Their model was able to capture the complex

relationship between microstructural heterogeneity and crack branching. The model was also able to replicate the widening fracture band with an apparent increase in fracture energy. Another notable work (Bleyer and Molinari 2017) described the fracture process as a 3D instability, which showed a strong dependence on the thickness of the sample. On the other hand, the branching pattern showed a strong dependence on the assumed internal length scale of PFM. To overcome this limitation of the internal length scale, a regularized phase field based cohesive model was introduced recently (Wu and Nguyen 2018; Wu 2017; Nguyen and Wu 2018). The model was able to capture multiple crack branching independent of internal length scale (Bleyer et al. 2017). However, the PFM seems to under-predict the crack velocity and the distinction between macro- and micro branching is rather arbitrary. Further, it is based only on one damage parameter, and it is unclear if it can handle mixed mode failures under general triaxial stress states (Nguyen et al. 2020). Thus overall, it is not as mature as the other aforementioned techniques, and also is computationally expensive. So further developments would be needed for general use in structural level commercial applications.

The smeared crack approach involving continuum damage mechanics (CDM) (Kachanov 1986) overcomes these limitations of the discrete approach. It naturally predicts branching (and merging) of cracks, accounts for stress triaxiality, and is easy to implement too. As a result, it is very commonly used for structural predictions of dynamic fracture in industry/academia. However, its effectiveness in predicting dynamic crack velocity evolution and branching is not fully established. The best modeling practices to obtain reliable predictions in this regard are also poorly understood. This poses a significant risk of developing inadequate designs.

To this end, this paper is aimed at examining the effectiveness of the CDM approach in predicting dynamic fracture, with a specific focus on crack velocity evolution, crack branching, and energy dissipation. Recently, benchmark evaluations with a similar motivation were presented in the excellent study by Wolff et al. (2015). They evaluated local and nonlocal damage models for dynamic fracture in PMMA via comparison to experiments from (Zhou 1996). The study provided an excellent benchmark for other numerical models. Their study emphasized the importance of nonlocality, and the damage initiation threshold strain. How-

ever, in many practical applications, the use of a non-local model is not always possible. This is because the treatment of the nonlocal weighting function near the structure boundary is not straightforward. Also, non-local models require a sufficiently small mesh size to capture the nonlocality, and can seriously compromise the computational efficiency of analyses for large-scale structures. Thus certain aspects of the local modeling approach deserve a closer examination. Primarily this includes the proper strain rate dependent scaling of the stress–strain law. Here this aspect is examined in detail. Further studies are pursued by considering important aspects, such as the mesh geometry and material viscoelasticity. We also interpret crack branching in terms of the crack velocity dependence of energy dissipation and fracture surface area. The essential objective is to fully understand the best practices for formulating local material point level damage models, to obtain accurate predictions of dynamic fracturing at the structure level.

## 2 Dynamic crack branching

### 2.1 Background

Crack branching is a key feature of dynamic fracture. Unlike quasistatic fracture, under higher strain rates, the localization of damage into one major crack is suppressed, leading to branching of cracks. In the simplest terms, this branching can be explained by the excess of available energy at the crack tip which cannot be dissipated by a single crack (Freund 1998; Sharon et al. 1995; Yoffe 1951).

A variety of experimental and analytical studies in the past have investigated conditions and criterion governing branching of a dynamically growing crack (Zhou 1996; Sharon et al. 1996; Fineberg 1997; Rabbi et al. 2019). This has led to several observations on salient behaviors in brittle materials which include:

1. Crack velocity evolution marked by acceleration to a steady state velocity
2. Relation of the steady state crack velocity to Rayleigh wave speed,  $c_R$
3. Crack branching above a certain threshold crack velocity
4. Mirror mist hackle patterns on fracture surfaces indicating crack acceleration
5. Nucleation of sister cracks at some distance away from the main crack

6. Linear dependence of the relative fracture surface area on the dynamic crack velocity etc.

Investigations by Ravi-Chandar and Knauss (Ravi-Chandar and Knauss 1984) have shown dynamic cracks to accelerate to a constant limiting velocity. They also found that micro-cracks can nucleate due to instabilities caused by high crack tip velocities. An archival finding in this regard is the Yoffe criterion for crack branching (Yoffe 1951). According to this criterion, crack branching is driven by the dynamic instability of the moving crack tip. The transition from a single crack to multiple cracks is obtained when the crack velocity exceeds 60 to 70% of the Rayleigh wave speed (Sharon et al. 1995; Abraham 2005). It is also evident from the experimental investigation of Fineberg and Marder (Fineberg and Marder 1999) that the fracture surface roughness depends on the crack velocity. Their investigation showed that the crack surface appears to be flat at low velocity and at high velocity, surface roughness from microvoids starts to appear. A coalescence of these microvoids in the fracture process zone creates dynamic instability and leads to micro-crack branching. Recent experimental investigations on a wide range of crack velocities have confirmed that the surface roughness increases during the constant velocity phase (Broberg 1996; Scheibert et al. 2012). These studies also revealed that the dynamic instabilities at the crack tip prevent the crack from further accelerating. Furthermore, there have been several studies showing the close dependence of the dissipated energy and relative fracture surface area on the crack velocity (Fineberg 1997; Sharon et al. 1995, 1996). It is essential to assess continuum scale numerical models for their predictions of these features (especially dynamic crack velocity and branching) to ensure the right prediction of energy dissipation.

### 2.2 Experimental benchmark

For the purpose of evaluating numerical results, the benchmark experimental results reported by Zhou (1996) on dynamic fracture of Polymethyl methacrylate (PMMA) plates will be used (similar to Wolff et al. (2015)). Their investigations were aimed at capturing the transition from a single localized crack to branched cracks. A dynamic crack was produced by applying a displacement preload  $\Delta u$  to the top and bottom edges of the PMMA plates, and then suddenly introducing a

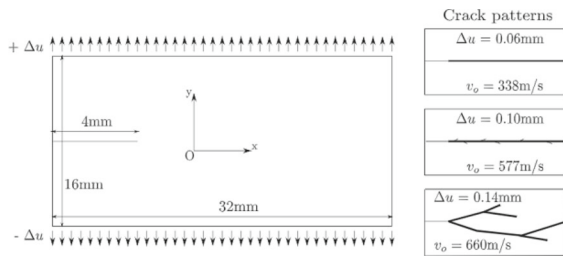


**Fig. 1** Schematics of the PMMA plate used for the numerical simulation. The right picture shows the crack patterns from the experimental investigation of Zhou (1996). Adapted from Wolff et al. (2015) with permission from John Wiley and Sons

pre-crack. Due to the preload, the suddenly introduced pre-crack propagated dynamically.

Results for three different preload values ( $\Delta u=0.06$  mm, 0.10 mm, and 0.14 mm) were reported. The crack velocities were measured using vertical electrical conductive lines which were bonded to the plate. For a preload of  $\Delta u=0.06$  mm one single crack was observed. Its path was straight, parallel to the precrack, and it propagated until the plate broke into two pieces. The corresponding crack velocity was 338 m/s. For  $\Delta u=0.1$  mm, the presence of micro-branching off the main crack was observed and the corresponding velocity of the main crack was 577 m/s. For  $\Delta u=0.14$  mm, extensive branching of the main crack was observed, and the leading major crack had a steady-state crack velocity of 660 m/s. These results are summarized in Fig. 1. Overall, for higher preloads, higher crack velocities and more branching can be observed. These tests will be simulated here using various local, continuum scale damage models.

### 3 Continuum damage model

PMMA being a homogeneous isotropic brittle solid, its failure is largely dominated by tensile failure (especially so in the tests considered here). So to capture its dynamic fracture we adapt an isotropic CDM model, similar to what was done in Wolff et al. (2015). We first present the strain rate independent behavior, and subsequently, strain rate dependence will be incorporated.

#### 3.1 Rate independent behavior

For an isotropic brittle solid, the elastic constitutive relation is described as,

$$\sigma_{ij} = C_{ijkl}\epsilon_{kl} \quad (1)$$

where  $i, j, k=1, 2, 3$ ,  $\sigma$  is the Cauchy stress tensor,  $\epsilon$  is the logarithmic strain tensor, and  $C$  is the fourth order elastic stiffness tensor given by,

$$C_{ijkl} = \lambda\delta_{ij}\delta_{kl} + \mu(\delta_{ik}\delta_{jl} + \delta_{il}\delta_{jk}) \quad (2)$$

where  $\lambda = E\nu/(1+\nu)(1-2\nu)$  and  $\mu = G = E/2(1+\nu)$  are the Lamé parameters,  $E$  is the Young's modulus,  $G$  is the shear modulus and  $\nu$  is the Poisson's ratio.

To capture damage, we introduce an isotropic damage model which consists of a scalar damage variable  $D$  that varies from 0 to 1. When  $D = 0$ , it denotes the original undamaged material, whereas  $D = 1$  represents the fully damaged state. The damage is introduced to the material by degrading the elastic modulus  $E$  as,

$$E = (1 - D)E^0 \quad (3)$$

where  $E^0$  is the original undamaged value of the modulus. The damaged value of  $E$  is then used to calculate the elasticity tensor of the damaged material via equation 2.

The damage variable,  $D$  is driven by a frame-invariant effective strain,  $\bar{\epsilon}$ , formulated as per Mazars model (Mazars 1986),

$$\bar{\epsilon} = \sqrt{\epsilon_i^2} \quad (4)$$

where  $\epsilon_i$  represent the principal strains ( $i = 1, 2, 3$ ). The evolution of the damage variable is formulated so as to produce a linear softening, i.e. a linear decrease in stress with increasing strain. In this framework, material degradation is assumed to be irreversible, and unloading occurs towards the origin. This is formulated as follows (Xue and Kirane 2019),

$$D = \begin{cases} 0 & \text{if } \bar{\epsilon} \leq \bar{\epsilon}_0 \\ \frac{\bar{\epsilon}_f}{\bar{\epsilon}_f - \bar{\epsilon}_0} \left[ 1 - \left( \frac{\bar{\epsilon}_0}{\bar{\epsilon}} \right) \right] & \text{if } \bar{\epsilon}_0 \leq \bar{\epsilon} \leq \bar{\epsilon}_f \\ 1 & \text{if } \bar{\epsilon}_f \leq \bar{\epsilon} \end{cases} \quad (5)$$

where  $\bar{\epsilon}_0$  is the value of effective strain at damage initiation and  $\bar{\epsilon}_f$  is the effective strain corresponding to complete damage. Under uniaxial tensile conditions,

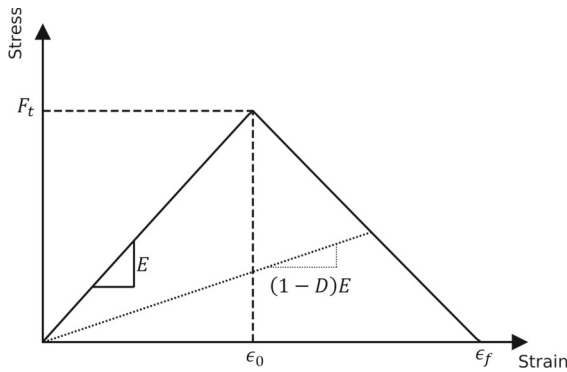


**Fig. 2** Material point stress–strain diagram with linear softening

the value of  $\bar{\epsilon}_0$  can be expressed in terms of the uniaxial tensile strength  $F_t$ , the Poisson's ratio  $\nu$  and elastic modulus  $E$  of the material as,

$$\bar{\epsilon}_0 = \frac{F_t}{E} \sqrt{1 + 2\nu^2} \quad (6)$$

We will refer to this model as the rate independent damage model or RIM. Generally for brittle materials, the strength and fracture energy is unequal under tensile and compressive loads. Usually this is accounted for by introducing an asymmetry in the damage initiation and completion strain thresholds (Pereira et al. 2015). However due to lack of data on compression damage (especially with rate effects), and the predominant focus on mode I tensile failures, here we assumed symmetric damage under tension and compression. We verified that the results were unaltered even after completely removing compression damage.

### 3.2 Characteristic length scale

This softening damage law needs to be equipped with a characteristic length scale, for which the simplest approach is the crack band model (CBM) (Bažant and Oh 1983; Bazant and Planas 1997; Červenka et al. 2005). In this approach, the slope of the post-peak softening branch is to be adjusted when the mesh size changes. This is done so that elements of varying sizes always dissipate energy consistent with the material's fracture energy. If this is not done, it is well established that mesh objectivity is lost.

The crack band approach can be easily combined with continuum damage mechanics. It is typically

implemented by introducing the element size  $h_e$  in the damage formulation by relating it to the failure strain as,

$$\bar{\epsilon}_f = \frac{2G_F}{F_t h_e} \sqrt{1 + 2\nu^2} \quad (7)$$

Here,  $h_e$  is the element size and  $G_F$  is the fracture energy, which is related to  $g_F$ , the area under the uniaxial stress vs strain curve by

$$G_F = g_F h_e \quad (8)$$

This approach has been proven to work for a wide variety of quasistatic fracture problems. However, recent findings (Gorgogianni et al. 2020) have shown that it works only when the damage pattern consists of clearly localized cracks. When the damage pattern is diffused (as can be expected for dynamic fracture), it fails to properly regularize the solution. To overcome this, a simple strategy is to choose a suitable element size  $h_e$ , which is small enough to be comparable or smaller than the crack band width  $h$ . The crack band width  $h$  is related to the size of material heterogeneity and can be obtained by measuring the minimum spacing of parallel tensile cracks  $s_{min}$  (Bažant and Pijaudier-Cabot 1989). If  $s_{min}$  is not known, it has to be chosen to be approximately of the order of the material heterogeneity. Then the damage model is calibrated to reproduce the desired fracture energy using this mesh size (i.e. as per Eq. 7). Following this, in all subsequent analyses, all element sizes must equal  $h_e$ . This simple approach is employed here too, to eliminate mesh effects. For varying element sizes within one model, a transitional localization parameter, as described in Gorgogianni et al. (2020) is necessary.

### 3.3 Strain rate dependence

The most important aspect to consider in material models for dynamic fracture is the time dependence of fracture propagation, which typically has two sources of material behavior:

1. The rate process of bond breaking at the crack tip which causes the damage evolution to be strain rate-dependent
2. Viscoelasticity of the bulk material



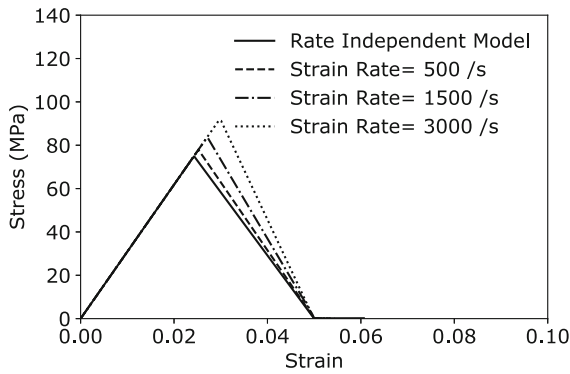


**Fig. 3** Material point stress–strain curve with damage delay method

The first point above is a feature of great interest for dynamic fracture (Le et al. 2018; Needleman 1988). It is manifested as an increasing strength and fracture energy with increasing strain rate (Le et al. 2018; Bazant and Planas 1997; John and Shah 1986; Bažant and Gettu 1992). In addition, at the structural level, effects of stress waves and inertia also become important, but most explicit dynamic finite element solvers automatically account for those.

### 3.3.1 Rate-independent failure strain

A rate dependent damage model which has a rate independent failure strain (i.e. strain at complete damage  $\bar{\epsilon}_f$ ) was employed by Ladeveze (1992), Allix and Deü (1997) and Pontiroli (1995). This approach is called the damage delay method or DDM. In this study, we adapt Pontiroli's formulation. Here the damage initiation strain  $\bar{\epsilon}_0$  is made a function of the strain rate, to match the increased strength with increased strain rate. However, the failure strain i.e. the complete damage threshold is kept rate independent. This is formulated as,

$$\bar{\epsilon}_{0,dyn} = \min \left[ \bar{\epsilon}_0 \left\{ 1 + \left( \frac{|\dot{\bar{\epsilon}}|}{a} \right) \right\}, 0.999\bar{\epsilon}_f \right] \quad (9)$$

$$\bar{\epsilon}_{f,dyn} = \bar{\epsilon}_f \quad (10)$$

where  $\bar{\epsilon}_{0,dyn}$  is the strain at which the failure initiates and  $a$  is the shape parameter that needs to be calibrated. Figure 3 shows the material point stress–strain curves for various strain rates for the DDM formulation. These correspond to  $a=34,000 \text{ s}^{-1}$  (calibration described later).

It can be seen that the strength (and fracture energy too) shows an increase with increasing strain rate. After the peak load is reached, the slope of the strain-softening branch changes to maintain the final damage threshold constant or rate independent. (The value of  $\epsilon_f = 0.05$ , corresponds to  $G_F = 300 \text{ N/m}$ ,  $F_t = 75 \text{ MPa}$ ,  $\nu = 0.35$  and  $h_e = 0.16 \text{ mm}$  whose choice is explained later).

This was also the formulation adapted in (Wolff et al. 2015) for their local modeling approach. However, upon closer inspection, it can be seen that this formulation remains stable only in a limited range of strain rates, since  $\bar{\epsilon}_f$  is rate independent, but not  $\bar{\epsilon}_0$ . So, beyond certain strain rates one can expect  $\bar{\epsilon}_0 > \bar{\epsilon}_f$  making the slope of the postpeak positive i.e. unstable. To avoid this, an artificial cap on the  $\bar{\epsilon}_{0,dyn}$  has to be introduced, as shown in Eq. 9. Thus, the DDM approach is viable as long as  $\bar{\epsilon}_0 < \bar{\epsilon}_f$ .

### 3.3.2 Rate-dependent failure strain

An alternative approach is considered here which overcomes this limitation. In this approach, the failure strain is also rate dependent. This approach has also been used in several studies e.g. Bazant and Li (1997) and proven to be effective. Here, this is formulated by adjusting the DDM formulation, to cause a radial shift in the stress–strain law, so that the slope of the softening branch does not change with increasing strain rate. To achieve this shift, the damage thresholds are modified as follows,

$$\bar{\epsilon}_{0,dyn} = \bar{\epsilon}_0 \left\{ 1 + \left( \frac{|\dot{\bar{\epsilon}}|}{b} \right) \right\} \quad (11)$$

$$\bar{\epsilon}_{f,dyn} = \bar{\epsilon}_f \left\{ 1 + \left( \frac{|\dot{\bar{\epsilon}}|}{b} \right) \right\} \quad (12)$$

where  $\bar{\epsilon}_{0,dyn}$  is the effective strain at which the damage initiates and  $\bar{\epsilon}_{f,dyn}$  is the effective strain corresponding to complete damage. Here,  $b$  is the shape parameter which needs to be calibrated. We will refer to this model as the radially scaled model or RSM.

Figure 4 shows the material point stress–strain curves at different strain rates for the RSM formulation with  $b=210,519.90 \text{ s}^{-1}$  (whose calibration is described later).

(The rate independent value  $\epsilon_f = 0.05$ , corresponds to  $G_F=300 \text{ N/m}$ ,  $F_t=75 \text{ MPa}$ ,  $\nu=0.35$ , and  $h_e=0.16 \text{ mm}$  whose choice is explained later). It is evident that the

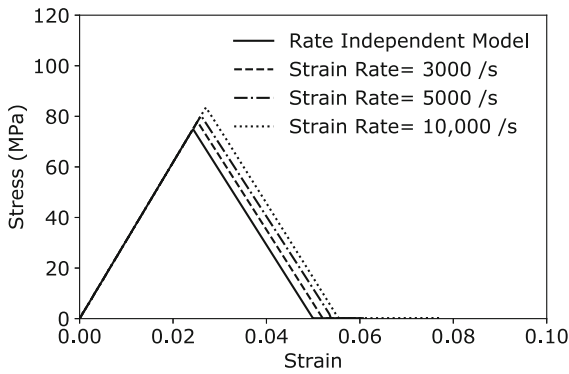


**Fig. 4** Material point stress–strain curve with radially scaled model

RSM formulation poses no limitation on the range of applicability of strain rates, since it ensures a negative postpeak slope for all strain rate values. Thus it has a clear advantage over the DDM.

### 3.3.3 Material viscoelasticity

The second source of rate dependence is the material viscoelasticity. A variety of studies in the past have investigated viscoelastic fracture (Willis 1967; Knauss 1970; Sluys et al. 1993; Schapery 1989). For polymers (including PMMA), it could become an important source of time-dependence in fracture (Bazant and Li 1997; Williams 1972; Wang et al. 2014; Rabbi and Chalivendra 2019; Fenghua et al. 1992). Here, the Maxwell model is used to account for the viscoelasticity of PMMA (Hernández-Jiménez et al. 2002; Jo et al. 2005; Graebling et al. 1993; Jia et al. 2007).

It uses a combination of spring and dash-pot to describe the time dependence of the elastic modulus. The spring in the Maxwell model is the Hookean element and its behavior is described by  $\sigma = K\epsilon$  which represents the elastic stretching of the material bonds. On the other hand, the Newtonian dash-pot describes the viscous behavior of the material and can be modeled as  $\sigma = \eta\dot{\epsilon}$ . Here  $\dot{\epsilon}$  is the strain rate and  $\eta$  is the viscosity. The ratio of viscosity to stiffness is the measure of the material’s viscoelastic response and is known as relaxation time,  $\tau$ .

In a generalized Maxwell model the applied strain is equal in each branches. So we can write,

$$\epsilon = \epsilon_j = \epsilon_j^s + \epsilon_j^d \tag{13}$$

where  $\epsilon^s$  and  $\epsilon^d$  indicates the strain in spring and dash-pot respectively. The total stress is the sum of stresses applied to each branch:

$$\sigma = \sigma_\infty + \sum_{j=1}^N \sigma_j \tag{14}$$

where subscript  $j$  indicates the  $j^{th}$  branch of the Maxwell model. The superposition principle and stress relaxation constant gives the stress at time  $t$ ,

$$\sigma(t) = \sigma_\infty + \sum_{j=1}^N \sigma_0 \exp\left(\frac{-t}{\tau_j}\right) \tag{15}$$

The elastic modulus of such a system can be written as,

$$E(t) = E_\infty + \sum_{j=1}^N E_0 \exp\left(\frac{-t}{\tau_j}\right) \tag{16}$$

Here we consider only a single Maxwell branch (which involves one spring and one dashpot in series). For such a system, the previous equation simplifies to,

$$E(t) = E_0 \exp\left(\frac{-t}{\tau}\right) \tag{17}$$

Here, the value of the relaxation time,  $\tau$  is taken as 766 s, as obtained from (Hernández-Jiménez et al. 2002). Figure 5 shows the generalized Maxwell model and material point stress–strain curve with viscoelasticity along with stress and strain histories in a relaxation test. From the figure, it is seen that the addition of viscoelasticity has not affected the stress–strain curve appreciably, even at a strain rate of 10,000/s. This is likely because the time scale under consideration is much smaller than  $\tau$ . So we do not expect it to affect the short term dynamic fracturing response considerably. Nevertheless, this will be verified.

## 4 Finite element modeling

### 4.1 Choice of element size

As pointed out previously, the issue of mesh objectivity is circumvented here by choosing an element size,

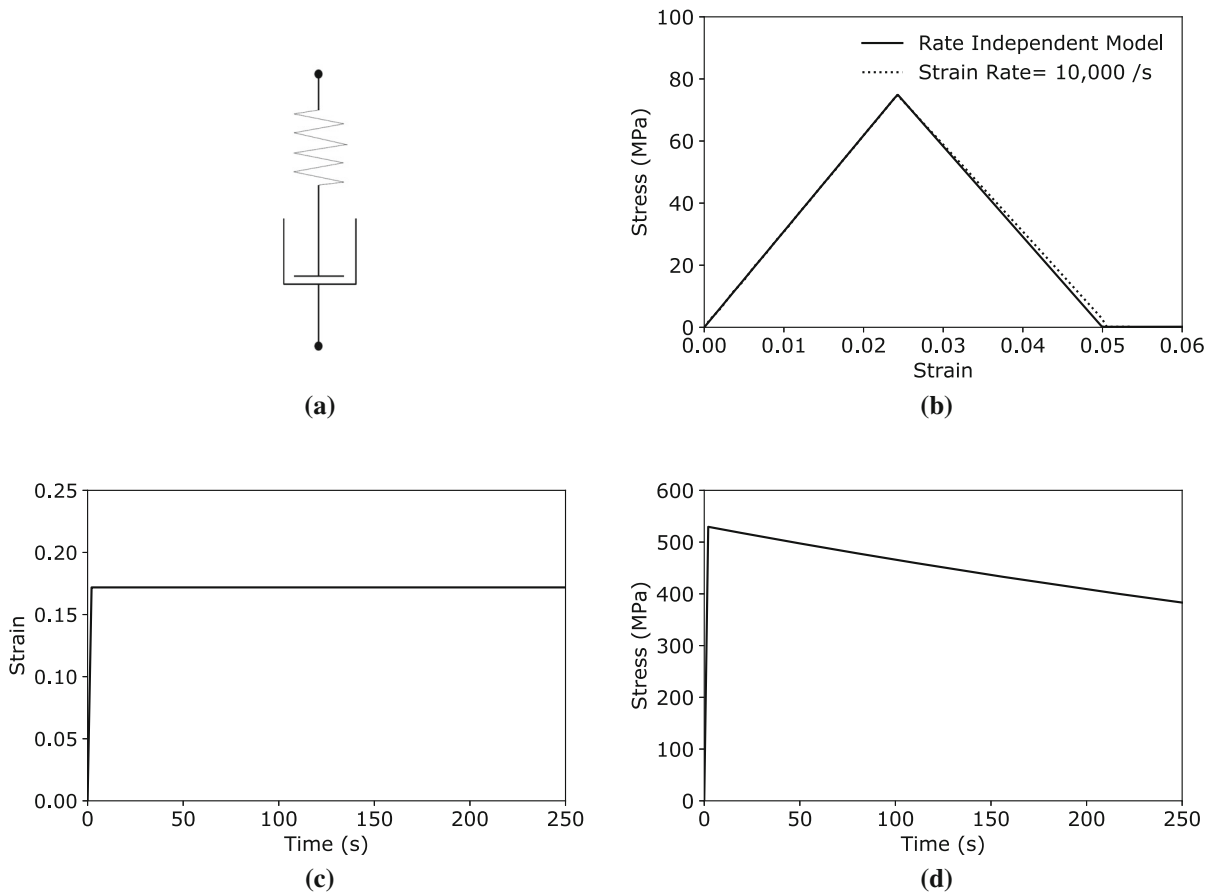


**Fig. 5** **a** Generalized Maxwell model, **b** material point stress–strain curve with viscoelasticity, **c** strain history, and **d** stress history in a relaxation test

calibrating the damage model with this size, and then using this mesh size in all models. The element size should ideally be comparable to the crack band width. It can be estimated to be comparable to the material heterogeneity size, or the minimum possible spacing  $s_{min}$  between parallel tensile cracks (Bažant and Pijaudier-Cabot 1989).

Since  $s_{min}$  is not known, an alternate consideration in choosing  $h_e$  is that the softening branch of the stress–strain curve at material point level should have a negative slope, i.e. the failure strain should be greater than the initiation strain. For the material properties for PMMA, it can be calculated that for  $h_e = 0.35$  mm,  $\epsilon_f = \epsilon_0$  indicating a vertical drop instead of softening. This sets the upper bound for element size. An element size equal to or larger than 0.35 mm would lead to unstable results (unless a transitional localization parameter suggested in Gorgogianni et al. (2020) is used.) A suitable assumption is  $\epsilon_f = 2\epsilon_0$  which ensures a negative

slope and leads to an element size of 0.16 mm or 160  $\mu\text{m}$ . It can be seen that this value of  $h_e$  is comparable to Irwin's characteristic length  $l_c = EG_F/F_t^2$ . From the material properties of PMMA summarized in Table 1,  $l_c$  turns out to be 0.1648 mm or 164.8  $\mu\text{m}$ .

## 4.2 Numerical implementation

The damage model was implemented in commercial FEA software Abaqus/Explicit using user-defined material subroutine VUMAT (Simulia 2017). The VUMAT subroutine is invoked at each material point  $k$  in each time increment. The FEA solver provides the strain increment  $\Delta\epsilon_{t,k}$  for each time increment,  $\Delta t$ . The incremental strain,  $\Delta\epsilon_{t,k}$  is then used to calculate the current strain  $\epsilon_{t,k}$  at each material point as well as the strain rate  $\dot{\epsilon}_{t,k}$  as:



**Table 1** Properties of the PMMA used in this study (Wolff et al. 2015; Hernández-Jiménez et al. 2002)

Properties	Values
Elastic modulus, $E$	3,090 MPa
Poisson's ratio, $\nu$	0.35
Density, $\rho$	1,180 kg/m <sup>3</sup>
Fracture energy, $G_f$	300 N/m
Ultimate strength, $F_t$	75 MPa
Relaxation time, $\tau$	766 s
Shape parameter, $a$	34,000 s <sup>-1</sup>
Shape parameter, $b$	210,519.90 s <sup>-1</sup>

$$\dot{\epsilon}_{t,k} = \frac{\Delta\epsilon_{t,k}}{\Delta t} \quad (18)$$

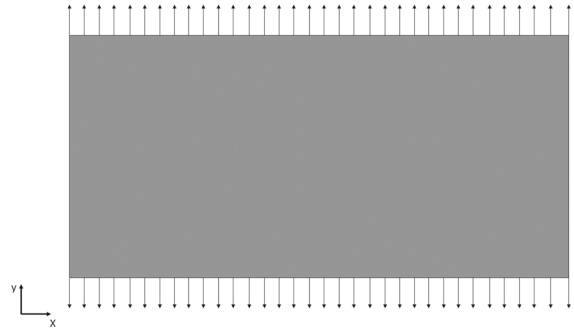
These are then used to obtain the damage increment  $\Delta d_{t,k}$  at that point, and finally the stress  $\sigma_{t,k}$  using the constitutive relation.

### 4.3 Specimen geometry and simulation steps

A finite element model of the PMMA plate of a 32 mm x 16 mm was built as shown in Fig. 6. The numerical simulations were carried out using a plane stress assumption. Dynamic fracturing was achieved by mimicking the steps of the experiments. In the first step, the PMMA-plate was stressed using constant displacement in the  $\pm y$  direction without the plate being constrained in any other direction. The displacement field without any damage was computed to satisfy static equilibrium.

In the next step, the previously calculated stress field was transferred and was used as an initial condition in the step file of the Abaqus/Explicit simulation. All material properties, boundary conditions, and meshing parameters were kept same for a successful transfer of these initial conditions to the second step of the analysis. In the second step, the damage model is activated after adding a straight pre-crack (of length 4 mm) in the structure. This pre-crack was created by deleting the corresponding elements. The stress concentration at the crack tip causes the growth of a dynamic mode-I crack in the structure, exactly as seen in the tests.

With this modeling strategy, a series of simulations were conducted on the PMMA plate. Primarily, the three different displacement preloads of  $\Delta u=0.06$  mm,  $\Delta u=0.10$  mm, and  $\Delta u=0.14$  mm were considered, sim-

**Fig. 6** PMMA plate used for dynamic crack propagation with prescribed displacement boundary condition on the top and bottom edges

ilar to the experiments. The predicted fracture pattern and crack velocity evolution are summarized and discussed in the following sections. Results are compared with the experimental investigation of Zhou (1996). Later on, additional preload cases are simulated, and the dissipated energy and fracture surface area predicted from the simulations are analyzed and compared with other experimental results by Sharon et al. (1996).

## 5 Results

### 5.1 Structured vs random mesh

The mesh which is generated by default in most commercial FEA software (such as Abaqus) for a rectangular geometry is a structured mesh, where all the mesh lines are parallel to one of the plate edges. However in local CDM models, the predicted fractures can tend to artificially propagate along the mesh lines, potentially hampering the prediction accuracy (Jirásek and Bauer 2012). This tendency is known as the directional mesh bias dependence. While the crack band model can alleviate the mesh size dependence, it remains highly prone to mesh bias dependence even for finer meshes, as shown by Jirásek and Grassl (2008). While complete elimination of mesh bias dependence appears impossible in a local damage model, a randomized unstructured mesh possessing no preferential path direction can considerably alleviate this issue, as shown in various studies (Leon et al. 2014; Bolander and Sukumar 2005; Ebeida and Mitchell 2011). For complete elimination of these effects a gradient based or a nonlocal model would be required. Here too, a randomized mesh

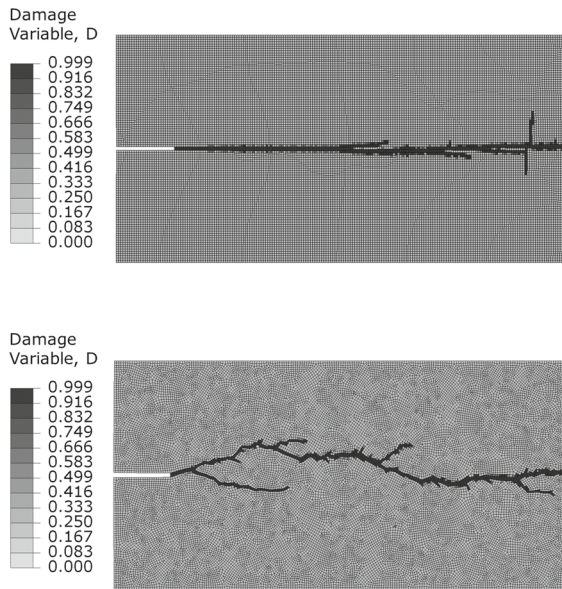


**Fig. 7** Fracture pattern obtained for the structured mesh (top image) and Crack pattern obtained for the non-structured mesh (bottom image)

with no apparent directional bias was found preferable, as shown next.

For this purpose, two meshes were created using 4-noded general-purpose shell elements (S4 in Abaqus), one structured and one random. In both cases, the element size was specified to be 0.16 mm  $\times$  0.16 mm. The meshes can be seen in Fig. 7.

With both these meshes, we proceed to predict dynamic cracking by the method described before. The rate independent damage model was used and the preload case of  $\Delta u = 0.06$  mm was simulated. The predicted fracture pattern was visualized by creating a contour plot of the damage variable  $D$  as shown in Fig. 7. From the plot for the structured mesh, it can be seen that crack branching is almost always predicted at right angles to the main crack. This is clearly an artifact of the mesh geometry and contrasts with many experimental observations, including the tests under consideration here. On the other hand, the random mesh predicted branching angles commonly seen in dynamic fracture experiments (Freund 1998; Zhou 1996). This clearly shows the advantage of using a random, unbiased mesh and therefore will be the chosen mesh for all subsequent analyses.

## 5.2 Rate independent analysis

The three preload cases were then simulated with the rate independent damage model (RIM), and the random mesh. The fracture pattern was obtained as before, by plotting the damage variable  $D$ . Secondly, the predicted crack velocity  $V_c$  was also analyzed in detail. For this purpose, a numerical methodology was developed, to mirror the experimental procedure of Zhou (1996). The fastest growing crack which propagated through the structure was considered as the main i.e. the leading crack. From the simulation results, in each time step, all damaged elements were identified and the coordinates of their centroid were extracted. Then, the instantaneous position of the main crack tip was identified as the highest x-coordinate of these centroids. These coordinate locations were then used to compute instantaneous crack velocity in X-direction at each time step using a MATLAB utility routine. (Since this was the velocity reported in the experimental and numerical benchmark study as well (Wolff et al. 2015; Zhou 1996).

The predictions from the rate independent damage model are shown in Fig. 8. For the smallest preload ( $\Delta u=0.06$  mm), one major crack is observed, which propagated horizontally. In addition, some macro-crack branches are observed. However, no branches were observed in the experimental study for this preload case. These macrocrack branches are seen to become much more prominent and denser for higher values of the preload, as shown in Fig. 8c, e. For these preloads ( $\Delta u=0.1$  mm and 0.14 mm) extensive crack branching is predicted. This is greatly in excess when compared to the experiments.

Figure 8b, d, and f show the velocity evolution of the main i.e. the leading crack ( $V_c$ ). It should be noted that the small drops in the velocity evolution plot correspond to instants when crack branching occurs. It can be seen that the model does predict an initial acceleration of the crack followed by the attainment of a steady state velocity. The model also predicts an increase in steady state velocity with an increase in preload. This agrees with experimental observations but only in a qualitative sense. The average predicted crack velocity ( $V_c$ ) is 477 m/s for preload  $\Delta u=0.06$  mm, 682 m/s for  $\Delta u=0.10$  mm, and 697 m/s for  $\Delta u=0.14$  mm. However, these velocities are much higher than measured in the experiments (338 m/s, 577 m/s, and 660 m/s).

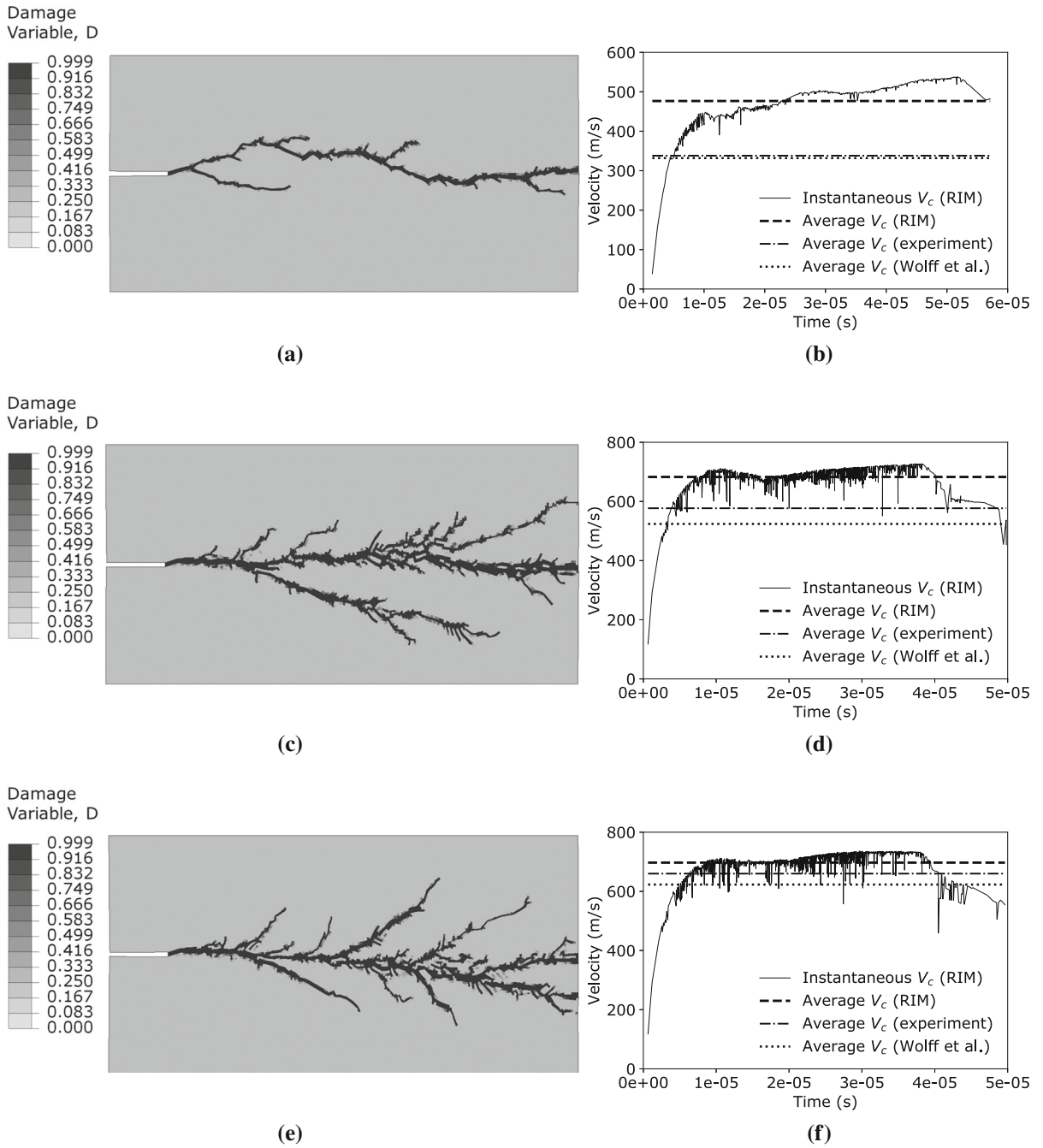


**Fig. 8** Fracture pattern and leading crack velocity ( $V_c$ ) evolution predicted by the rate independent damage model (RIM) for preloads of **a, b**  $\Delta u = 0.06$  mm, **c, d**  $\Delta u = 0.10$  mm, and **e, f**  $\Delta u = 0.14$  mm

Further, the extent of branching is also much greater than observed.

This is due to the fact that the energy dissipated by each material point is limited to the rate independent, static fracture energy value. Thus, to dissipate the excess available energy, the predicted fractures must extensively branch. Thus it appears that for a better quantitative agreement with the tests, incorporating strain rate dependence is necessary.

### 5.3 Damage delay method (DDM)

The analyses are now repeated by introducing rate dependence in the damage model, via the damage delay method i.e. DDM. Unlike the rate independent damage model, an additional material parameter i.e. the shape parameter  $a$  is required. It is calibrated similar to the method in Wolff et al. (2015) by matching the predicted velocity  $V_c$  for the smallest preload case ( $\Delta u = 0.06$  mm). The calibrated value of  $a$  turned out to be  $34,000 \text{ s}^{-1}$  which yielded a velocity  $V_c$  of  $344 \text{ m/s}$ , matching fairly well with the experimental crack velocity =  $338 \text{ m/s}$ .

The results for all three preloads are shown in Fig. 9. It can be seen that the extent of fracturing for each case is decreased compared to the RIM, and agrees better with experiments to a certain extent. For  $\Delta u=0.06$  mm one major crack with little to no branching is observed, similar to tests. However for the intermediate case of  $\Delta u=0.1$  mm considerable macrobranching is observed, which was not seen in the tests. For the case of  $\Delta u=0.14$  mm, the extent of macrobranching seems to agree with the tests. The predicted average crack velocities ( $V_c$ ) were  $344 \text{ m/s}$ ,  $584 \text{ m/s}$ , and  $628 \text{ m/s}$  for the three preloads, which agree well with the measured values of  $338 \text{ m/s}$ ,  $577 \text{ m/s}$ , and  $660 \text{ m/s}$ .

Thus the incorporation of DDM decreased the predicted crack propagation velocity as well as the extent of fracturing when compared to the rate independent formulation. The steady state average velocity of the primary crack agrees well with the test data. However, the extent of macro-crack branching is overpredicted.

### 5.4 Radially Scaled model (RSM)

The three preload cases were then simulated with the radially scaled damage model (RSM). Similar to DDM,

the shape parameter  $b$  needs calibration. It is calibrated similar to before, by matching the predicted velocity for the smallest preload case ( $\Delta u = 0.06$  mm). The calibrated value of  $b$  turned out to be  $210,519.90 \text{ s}^{-1}$  which yielded a velocity ( $V_c$ ) of  $341 \text{ m/s}$ , matching fairly well with the experimental crack velocity =  $338 \text{ m/s}$ . The predictions are shown in Fig. 10. It is found that the results obtained (on the fracture pattern) are qualitatively rather different from the previous ones.

For  $\Delta u = 0.06$  mm, the RSM formulation predicts a single straight crack which agrees well with the experiments. For higher preloads, an interesting behavior is observed. Unlike the DDM, extensive microbranching is predicted, to such an extent that the entire fracture pattern appears like a thickened band. This is very similar to the experiments, and also, the results from Wolff et al. (2015). However, the microbranching does appear to be overpredicted than experiments. Further, for  $\Delta u=0.14$  mm, a similar thickened fracture band is predicted, which then branches, leading to two thick bands. This branching of the thick bands is viewed here as “macro-branching”. However, the formed macrobranches do not further rebranch as seen in the tests. Thus, this model overpredicts microbranching, but underpredicts macrobranching. The predicted average crack velocities ( $V_c$ ) are  $341 \text{ m/s}$ ,  $557 \text{ m/s}$ , and  $623 \text{ m/s}$  which agree well with the measured values of  $338 \text{ m/s}$ ,  $577 \text{ m/s}$ , and  $660 \text{ m/s}$ . The velocity increases before the crack branching and a sharp instantaneous drop in velocity is observed when crack branching occurs, after which the velocity returns to the steady state value.

Overall, it is found that the radially scaled damage model has an edge over the damage delay method. The agreement from RSM is slightly better with the experimental data. While the DDM underpredicts microbranching and overpredicts macrobranching, the RSM overpredicts microbranching and underpredicts macrobranching. However the RSM approach is applicable to all values of strain rates, unlike the DDM, and therefore should be the preferred strategy for incorporating rate dependence in damage models. In general, considering the quantitative results on crack velocities and energy dissipation are more helpful in deciding which results are more realistic. However, analyzing the fracture patterns can provide a qualitative picture, proving to be valuable in aiding the quantitative conclusions. This is found especially true here, which shows a dramatic difference in the predictions caused by changing

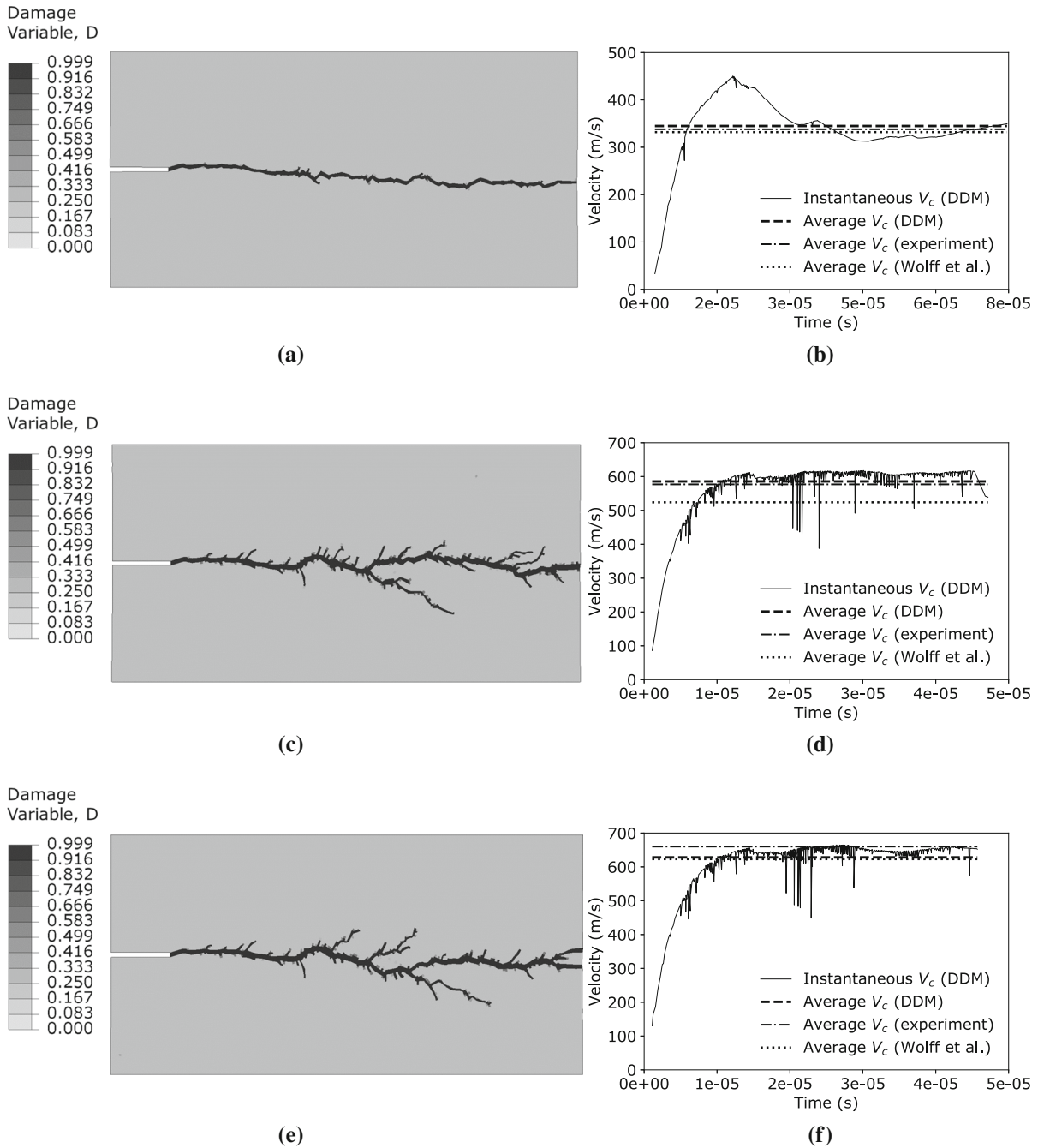


**Fig. 9** Fracture pattern and leading crack velocity ( $V_c$ ) evolution predicted by the damage delay method for preloads of **a, b**  $\Delta u = 0.06$  mm, **c, d**  $\Delta u = 0.10$  mm, and **e, f**  $\Delta u = 0.14$  mm



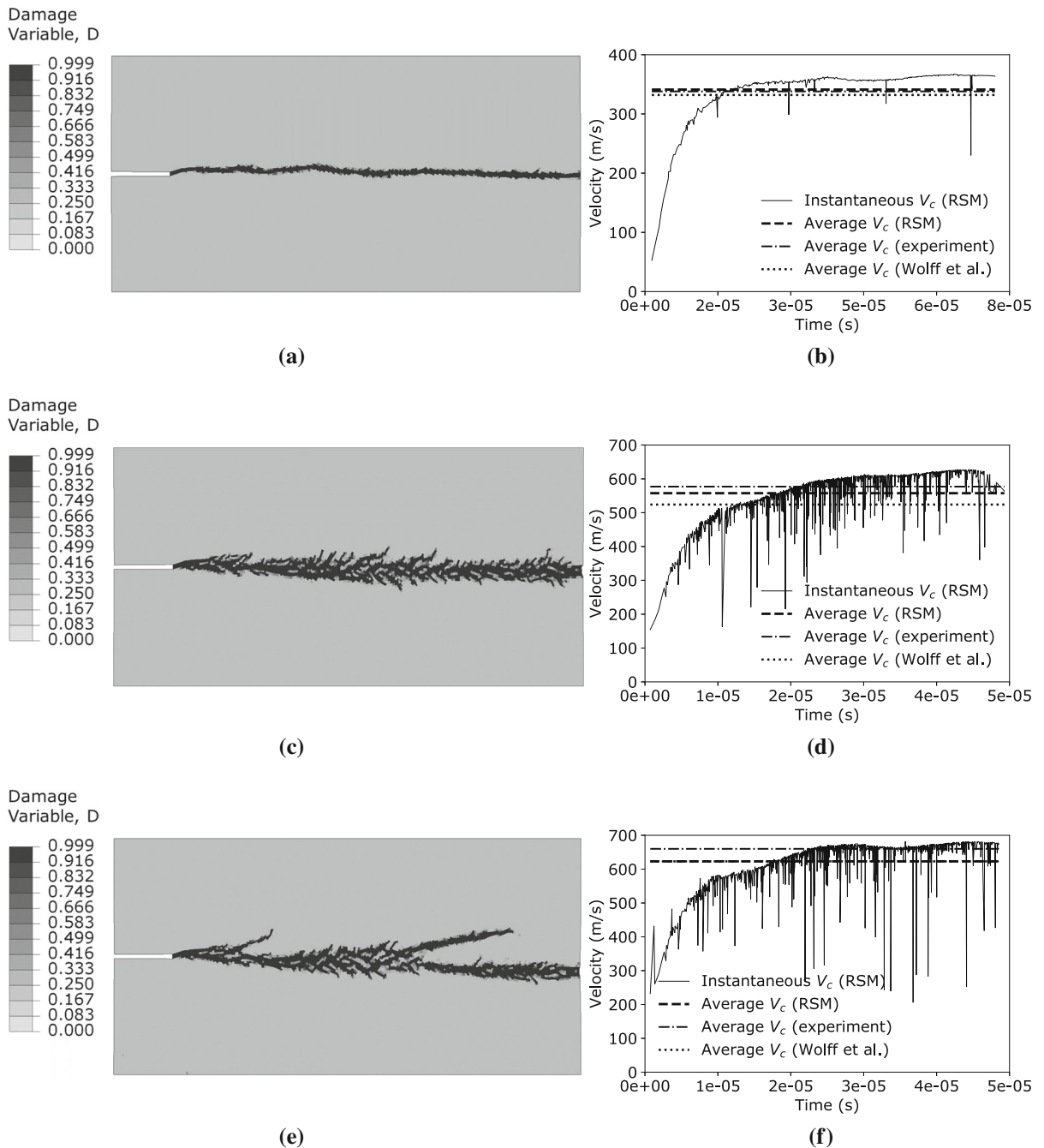


**Fig. 10** Fracture pattern and leading crack velocity ( $V_c$ ) evolution predicted by the radially scaled model for preloads **a, b**  $\Delta u = 0.06$  mm, **c, d**  $\Delta u = 0.10$  mm, and **e, f**  $\Delta u = 0.14$  mm



the manner of scaling the stress–strain damage law. Overall, the local damage model is found to capture various finer features of dynamic fractures.

### 5.5 Effect of material viscoelasticity

As discussed before, material viscoelasticity did not have a significant effect on the stress–strain curve. Nevertheless, we evaluate its effect on dynamic fracture predictions, when used in conjunction with the RSM formulation. The three preload cases were simulated accordingly. Figure 11 shows the predicted fracture pattern and crack velocities. These results look very similar to those obtained from RSM without viscoelasticity. The predicted velocities ( $V_c$ ) for the three preload cases are 349 m/s, 554 m/s and 610 m/s, which again did not alter appreciably. This suggests that for dynamic fracture of PMMA, viscoelasticity is not a critical effect and need not be included in material models. This is likely due to the relaxation time constant of 766 seconds, which is much longer than the total crack propagation times. Viscoelasticity will be important for longer term fracture problems such as creep and fatigue, but not for short term dynamic fracture.

### 5.6 Initial damage threshold

The results in Wolff et al. (2015) also indicated a disagreement with experiments in terms of extent of branching. As a potential remedy, they suggested introducing a strain rate threshold, below which the response is strain rate independent. Here too, it is seen that the RSM approach underpredicted the macrocrack branching for the large imposed displacement ( $\Delta u=0.14$  mm). This is likely due to the overprediction of microbranching.

Hence, in this section, we investigate if raising the strain rate threshold affects the results. This is formulated as,

$$\bar{\epsilon}_{0,dyn} = \max \left[ \bar{\epsilon}_0 \left\{ 1 + \left( \frac{|\dot{\epsilon}|}{a} \right) \right\}, \bar{\epsilon}_{0,init} \right] \quad (19)$$

For this study, we consider the initial damage threshold,  $\bar{\epsilon}_{0,init}$  to be 0.030 and 0.040. Figure 12 shows the predicted fracture pattern and crack velocity. In both cases, raising the initial damage threshold reduced the extent

of microbranching, and slightly increased the macrobranching. The average crack velocity ( $V_c$ ) however decreased to 603 m/s and 599 m/s for  $\bar{\epsilon}_{0,init} = 0.030$  and 0.040 respectively. Thus adjustment of the damage initiation threshold, did aid in reducing the microbranching, but at the cost of greater errors in crack velocity.

### 5.7 3D crack branching simulations

Crack branching was described by Bleyer and Molinari (2017) as a 3D instability and their work showed the impact of structural thickness on crack branching. To verify if the 2D plane stress assumption was valid, here two of the analyses were repeated with a full 3D model. Similar to before, a 3D domain with dimensions of 32 mm  $\times$  16 mm  $\times$  0.16 mm was created. All the other modeling parameters, viz. material properties, and boundary conditions were kept the same. The damage model with the highest preload case ( $\Delta u = 0.14$  mm) was simulated using DDM and RSM and the results are shown in Fig. 13. The leading crack velocity  $V_c$  evolution and the degree of crack branching are largely similar to 2D simulations. It shows an initial acceleration followed by the attainment of a steady-state value. The fracture pattern for DDM formulation shows extensive macrobranching with little microbranching. On the other hand, the RSM formulation predicts, like before, a dense band of fracturing with substantial microbranching and little macrobranching.

## 6 Additional analyses

The results so far suggest that the best results were obtained with the RSM formulation, which we now evaluate further. Additional simulations were performed using the RSM formulation for preloads equal to 0.08 mm, 0.12 mm, and 0.16 mm to observe the predicted fracture patterns and corresponding crack velocities. Results that are largely consistent to before were observed. E.g. for  $\Delta u=0.08$  mm, a mostly straight crack with some micro-branches was observed with an average crack propagation velocity ( $V_c$ ) of 488 m/s (which is intermediate to  $\Delta u=0.06$  mm and  $\Delta u=0.1$  mm). For  $\Delta u=0.12$  mm, a diffused crack with macro-branches is obtained for an applied displacement of 0.12 mm with an average crack velocity ( $V_c$ ) of 581 m/s and finally,

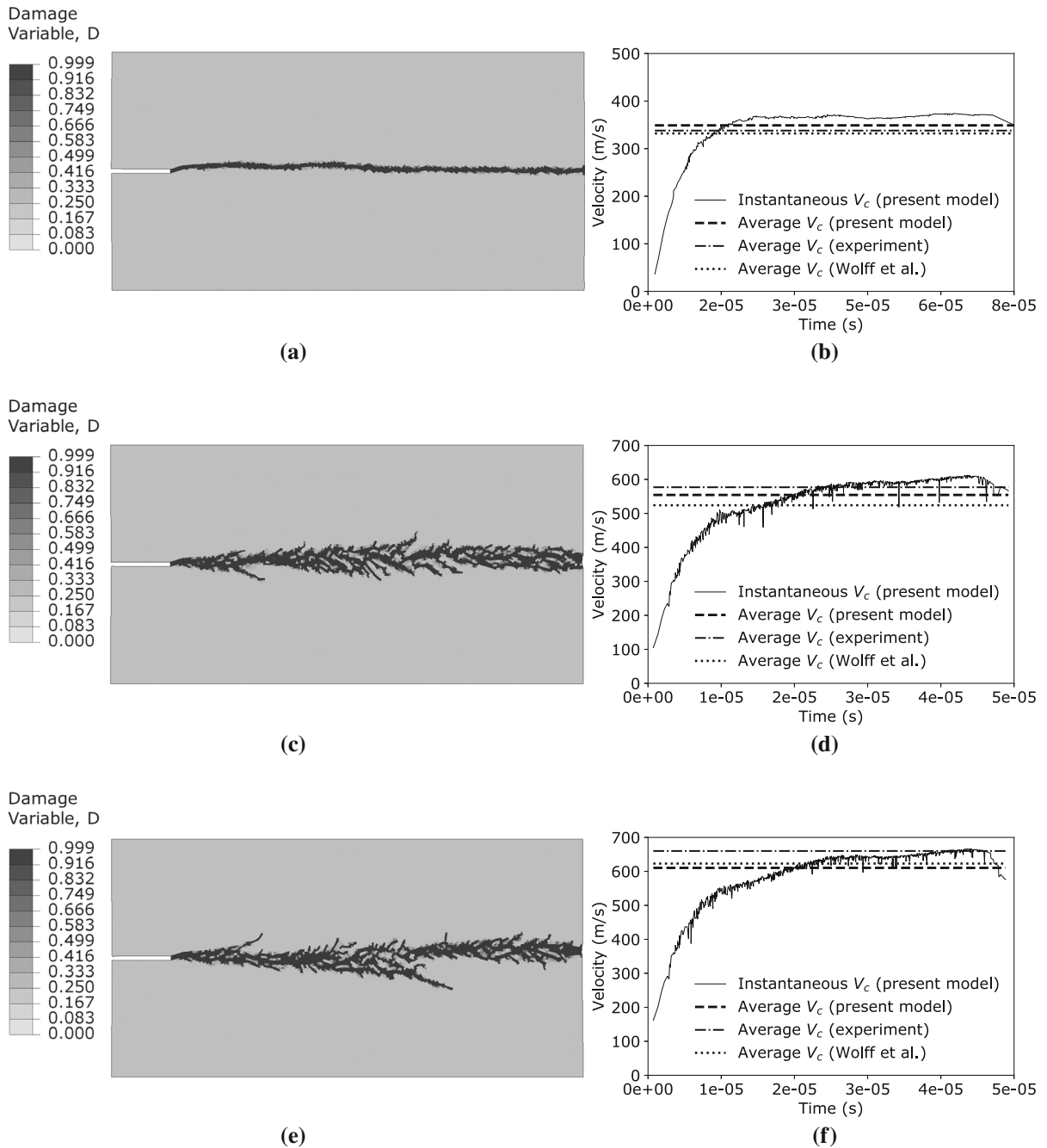


**Fig. 11** Fracture pattern and leading crack velocity ( $V_c$ ) evolution predicted by the radially scaled model implemented with viscoelasticity, for preloads of **a, b**  $\Delta u = 0.06$  mm, **c, d**  $\Delta u = 0.10$  mm, and **e, f**  $\Delta u = 0.14$  mm

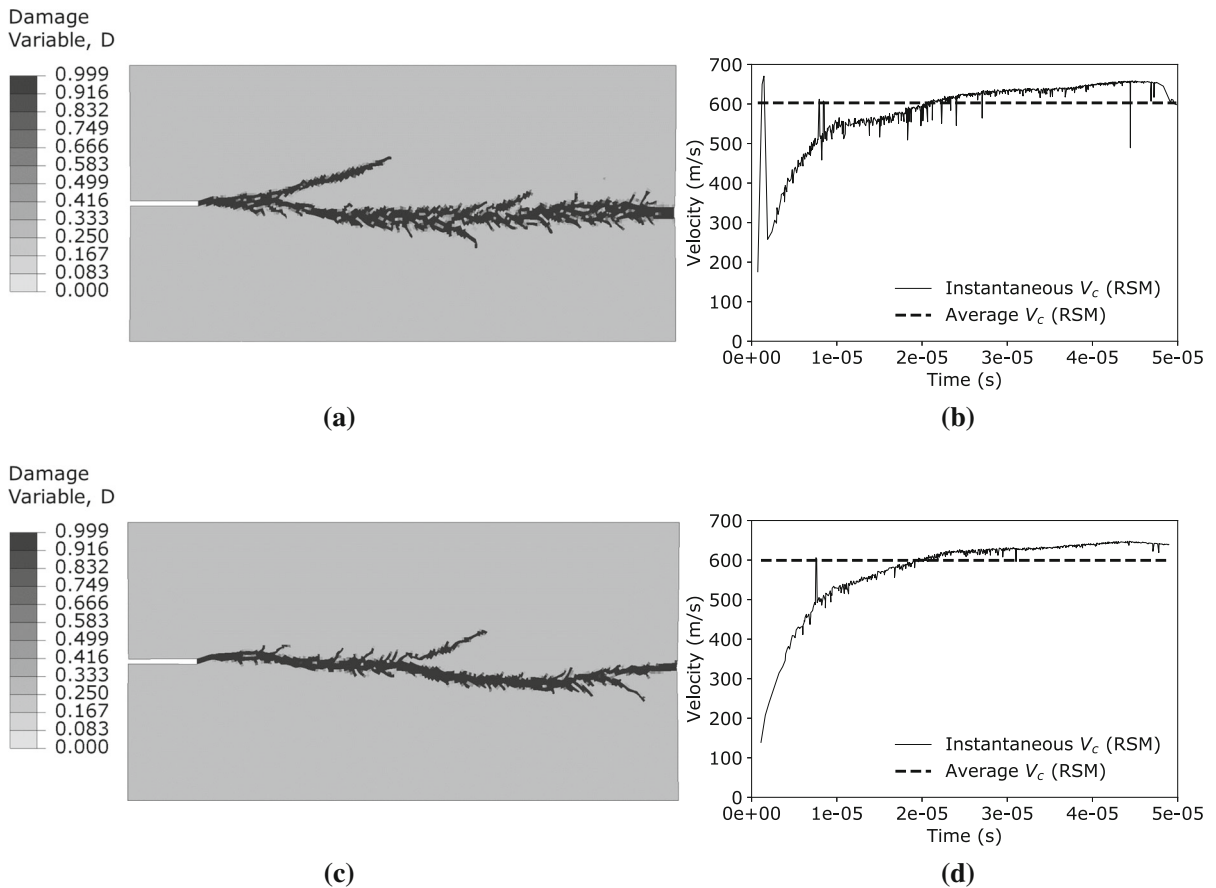


**Fig. 12** Fracture pattern and leading crack velocity ( $V_c$ ) evolution predicted with the initial damage threshold **a**,  $\bar{\epsilon}_{0,init} = 0.030$ , and **c**,  $\bar{\epsilon}_{0,init} = 0.040$

for  $\Delta u = 0.16$  mm an even more intricate pattern of cracks with extensive branching is predicted with an average crack velocity ( $V_c$ ) of 649 m/s. In addition to the main crack and macro-crack around the main crack, two more cracks also appeared near the boundary of the structure due to high-stress concentration in those regions as can be seen in Fig. 14e. These results fit well with the previous predictions and are now collectively analyzed further.

### 6.1 Dissipated energy

Experimental measurements in the past have suggested that the dissipated fracture energy during dynamic fracture increases with increasing crack velocity (Sharon et al. 1996). The predictions from the RSM analyses were evaluated for this aspect too. Similar to Wolff

et al. (2015) and Sharon et al. (1996), the dissipated energy was calculated from the strain energy as,

$$U = \frac{1}{2} \int_0^D \underline{\epsilon}^T \cdot \underline{C} \cdot \underline{\epsilon} \cdot dD \tag{20}$$

The total fracture energy dissipated by the structure then can be calculated by,

$$G_c = \frac{U}{l} \tag{21}$$

where  $l$  is 28 mm.

Figure 15 shows the dissipated fracture energy as a function of average crack velocity for different models used in this study. It is clear that more energy is dissipated as the crack velocity is increased. The simulation results from RSM show a close agreement with the

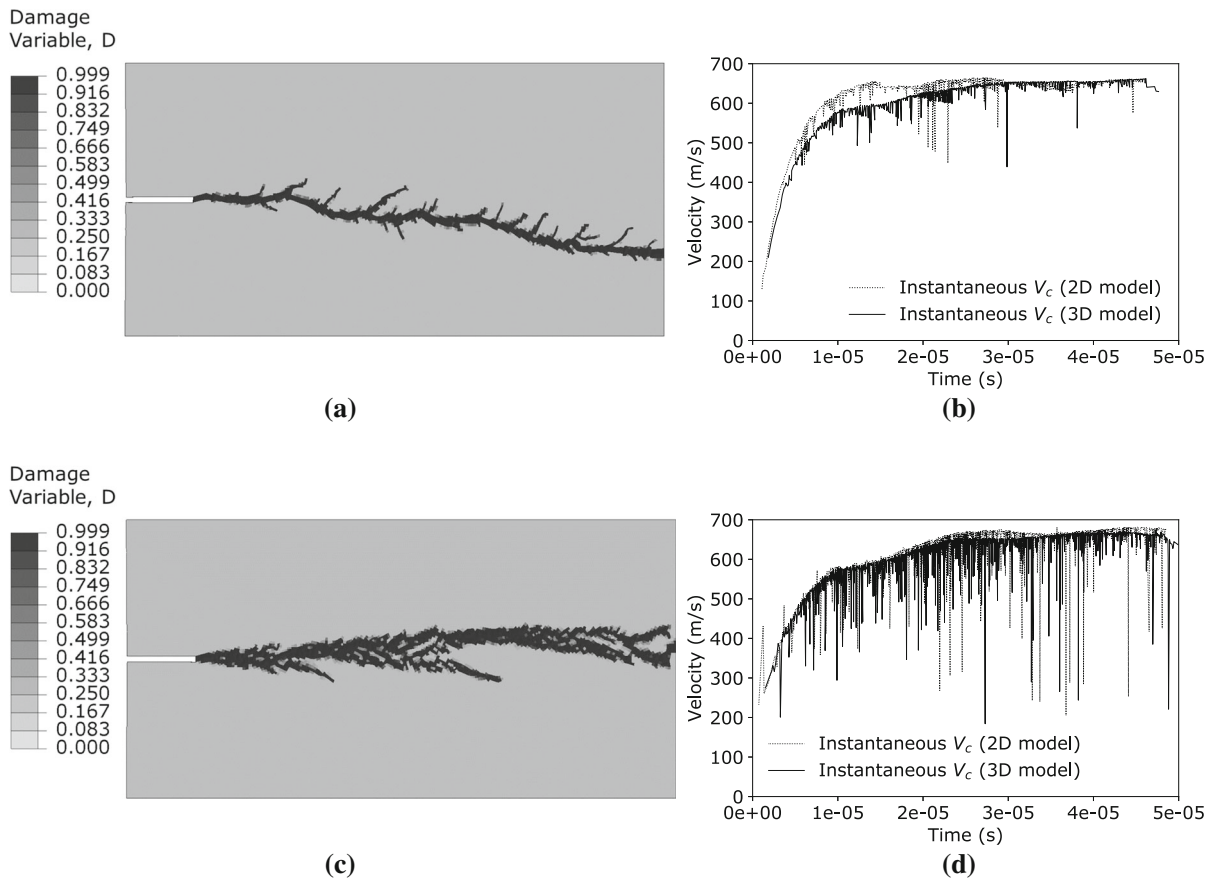


**Fig. 13** Fracture pattern predicted using a 3D model with **a** DDM formulation and **c** RSM formulation; Comparison of the leading crack velocity ( $V_c$ ) evolution predicted by 2D and 3D models, **b** DDM formulation, **d** RSM formulation

experimental outcome of Sharon et al. (1996). However, the RIM and DDM formulation under-predict the dissipated energy for higher crack velocities. This suggests that the RSM formulation is most consistent in terms of energy dissipation for a broad range of crack velocity values. The increase in fracture energy with strain rate, in the DDM approach is likely not adequate.

## 6.2 Relative surface area

Another aspect of dynamic fracture, emphasized in Sharon et al. (1996) is the relative surface area as a function of crack velocity. This is an effective way to observe the increased crack branching with increasing crack velocity. This is defined as the ratio of the total fracture area created, to that created by a single straight

crack. (Thus a value of one indicates no branching, and greater the value, more the branching). In Sharon et al. (1996) a linear relationship between this ratio and the corresponding steady state crack velocity was found. In this study, these calculations were performed for the predictions for all three modeling approaches (i.e., RIM, DDM, and RSM). The results are plotted in Fig. 16.

It can be seen that the models indeed capture the increase in fracture surface area with increasing crack velocity. Moreover, the relationship is seen to be linear, consistent with the experiments. It is seen that for RSM formulation as the velocity reaches close to 650 m/s, the amount of surface created due to branching reaches over four times the surface formed by a sharp single crack.

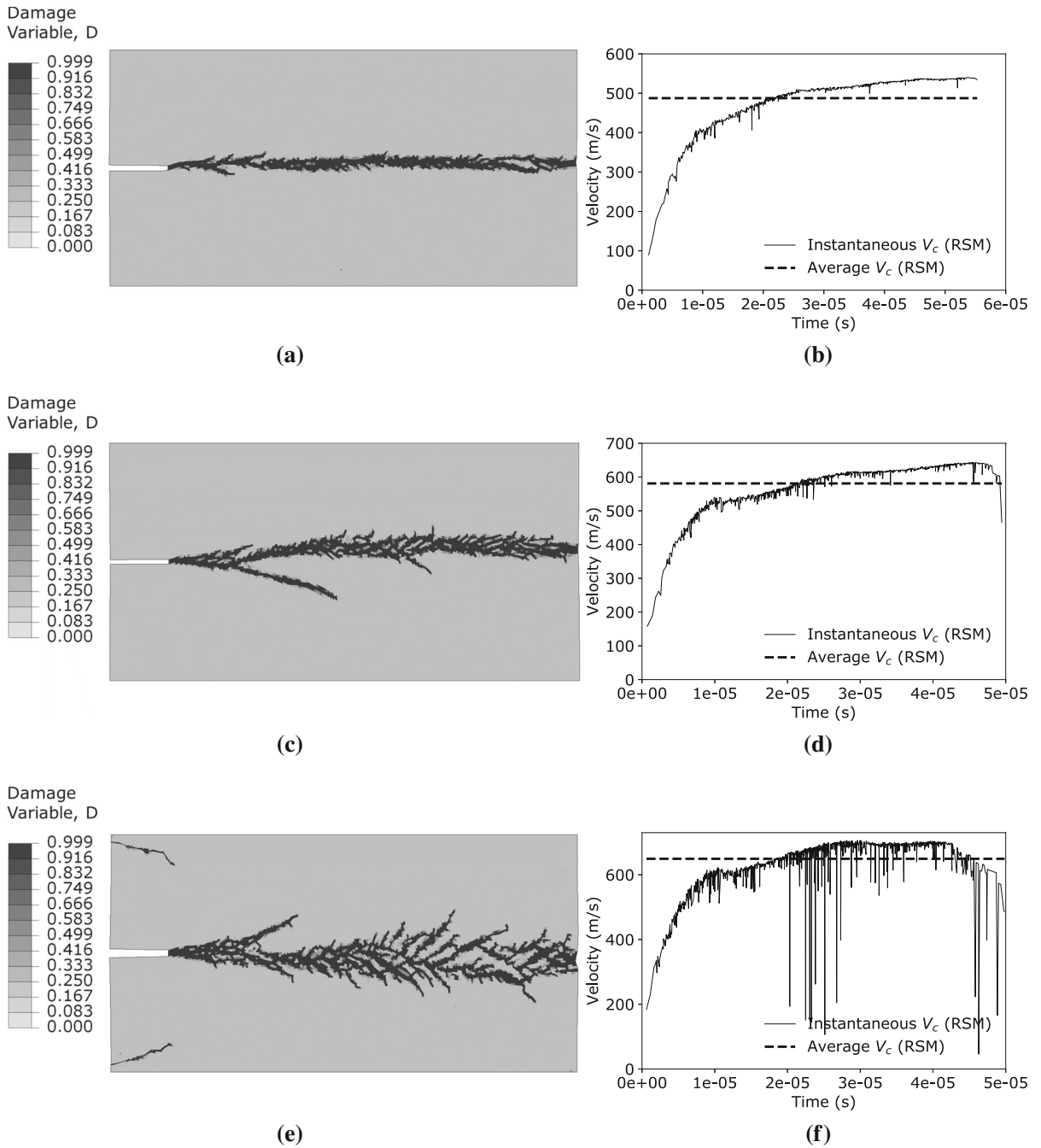


**Fig. 14** Fracture pattern and leading crack velocity ( $V_c$ ) evolution predicted by the radially scaled model for preloads of **a, b**  $\Delta u = 0.08$  mm, **c, d**  $\Delta u = 0.12$  mm, and **(e, f)**  $\Delta u = 0.16$  mm

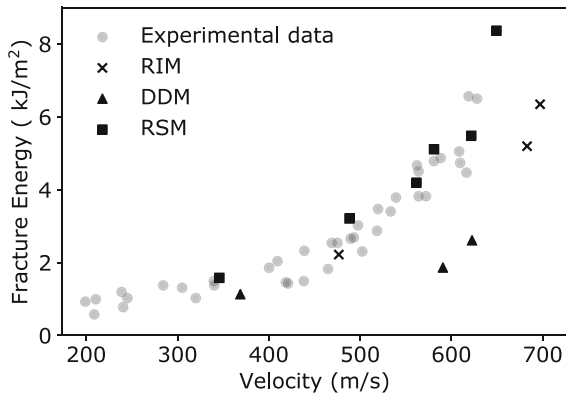


**Fig. 15** Dissipated fracture energy compared to the experimental data of Sharon et al. (1996)

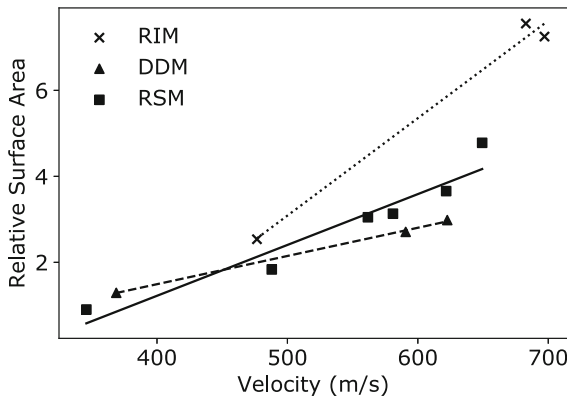


**Fig. 16** The surface area formed per unit crack extension as a function of average crack velocity

### 6.3 Crack branching criterion

The macro-crack branching predicted here is analyzed further and compared to the Yoffe instability criteria (Yoffe 1951). According to this criterion, for a high speed crack propagating normal to the maximum tensile stress, there is a critical velocity (70% of the Rayleigh wave speed (Abraham 2005)), above which the crack tends to become unstable and branches. Beyond this critical velocity, the mean acceleration of the crack decreases and the crack velocity starts to oscillate. This oscillation leads to the dynamic instability of the moving crack tip and the main crack sprouts side branches in the structure.

For PMMA under consideration, the shear wave speed  $c_S (= \sqrt{G/\rho}) = 984.81$  m/s. Then, the Rayleigh

wave speed  $c_R$  is given by Freund (1998)

$$c_R = c_S \frac{0.862 + 1.14\nu}{1 + \nu} \quad (22)$$

This computes to 919.89 m/s. Here, macro-crack branching was obtained when the crack velocity reached 660 m/s which is nearly 71% of  $c_R$  which agrees remarkably well with the Yoffe instability criterion. This suggests that as long as the damage model embodies the right strain rate dependent fracture energy, the crack branching instability can be automatically captured and that it is not essential to really capture local crack tip stresses and strains. This agrees with findings of a similar nature, but at the molecular scale (Abraham 2005).

## 7 Conclusions

This work presents a detailed numerical investigation of the predicted dynamic crack propagation and branching in a brittle material, using various local, rate dependent continuum damage models. The models were used to predict the fracture pattern, crack velocity, branching, and energy dissipation in a pre-cracked 2D PMMA plate loaded under tension. The results were compared to experimental data as well as previous modeling results from Wolff et al. (2015). The main conclusions are as follows:

1. A local damage mechanics based model can capture many aspects of dynamic fracture. This includes crack acceleration to a steady state velocity and increased crack branching with increased crack velocity
2. A rate independent damage model considerably overpredicts the dynamic crack velocity and the extent of fracturing. This implies that incorporating fracturing rate effects is a must for dynamic fracture analyses of brittle materials like PMMA
3. Incorporating the fracturing rate effects, by making the strength and fracture energy rate dependent improves the predictions significantly
4. Two ways of incorporating fracturing rate effects were evaluated here viz, the damage delay method (DDM) and the radial scaling method (RSM). In the former, the strain at complete damage, is rate independent, causing the post peak slope to be rate independent. On the other hand, in the latter, the strain



at complete damage is rate dependent, such that the post peak slope is rate independent. Both the DDM and RSM approaches predict crack velocities well. But the DDM approach underpredicts microbranching and overpredicts macrobranching. On the other hand, the RSM approach overpredicts microbranching and underpredicts macrobranching. However, the RSM approach does a better job of capturing the dependence of energy dissipation on crack velocity. Also it is applicable to all strain rate values, unlike the DDM. This gives the RSM approach an appreciable edge over the DDM.

5. The models capture the linear dependence of the relative fracture surface area on crack velocity.
6. The predicted macrocrack branching is found to occur in agreement with the Yoffe instability criterion. This suggests that the branching instability can be captured by CDM based approaches with smeared crack representations
7. A random bias free mesh is seen to work best to predict dynamic crack branching angles and overall fracture patterns
8. Viscoelasticity of the bulk PMMA was found to play a negligible role in the predictions and can be ignored

It is emphasized that the results are only valid if the mesh size is kept constant within the model. This is because the damage pattern can transition from localized to diffused during dynamic fracture. So, if the mesh size is changed within the model, objectivity would be lost even if the postpeak slope is adjusted as per the crack band approach, as recently explained in Gorgogianni et al. (2020). These issues can be addressed by using a transitional localization parameter or by adapting a nonlocal model. Further, for heterogeneous materials such as concrete, it was shown that material comminution effects should be considered to correctly capture the energy dissipation at ultra high strain rates ( $10^4$  to  $10^6$ /s) (Luo et al. 2019; Bažant and Caner 2014; Kirane et al. 2015). However, given the overall agreement with experimental data, it was not deemed necessary here. Including these effects might become necessary at higher strain rates, and should be investigated.

**Acknowledgements** Research was sponsored by the Army Research Office and was accomplished under Grant number W911NF-19-1-0312. The views and conclusions contained in this document are those of the authors and should not be inter-

preted as representing the official policies, either expressed or implied, of the Army Research Office or the US Government. The US Government is authorized to reproduce and distribute reprints for Government purposes notwithstanding any copyright notation herein.

#### Declaration

**Conflict of interest** The authors declare that they have no conflict of interest.

#### References

- Abraham FF (2005) Unstable crack motion is predictable. *J Mech Phys Solids* 53(5):1071
- Allix O, Deü JF (1997) Delayed-damage modelling for fracture prediction of laminated composites under dynamic loading. *Eng Trans* 45(1):29
- Barenblatt GI et al (1962) The mathematical theory of equilibrium cracks in brittle fracture. *Adv Appl Mech* 7(1):55
- Bažant ZP, Caner FC (2014) Impact comminution of solids due to local kinetic energy of high shear strain rate: I. Continuum theory and turbulence analogy. *J Mech Phys Solids* 64:223
- Bažant ZP, Gettu R (1992) Rate effects and load relaxation in static fracture of concrete. *ACI Mater J* 89(5):456
- Bazant ZP, Li YN (1997) Cohesive crack with rate-dependent opening and viscoelasticity: I. mathematical model and scaling. *Int J Fract* 86(3):247
- Bažant ZP, Oh BH (1983) Crack band theory for fracture of concrete. *Mat Construct* 16(3):155
- Bažant ZP, Pijaudier-Cabot G (1989) Rate-dependent scaling of dynamic tensile strength of quasibrittle structures. *J Eng Mech* 115(4):755
- Bazant ZP, Planas J (1997) Fracture and size effect in concrete and other quasibrittle materials, vol 16. CRC Press, Boca Raton
- Bazant ZP, Planas J (1997) Fracture and size effect in concrete and other quasibrittle materials, vol 16. CRC Press, Boca Raton
- Bleyer J, Molinari JF (2017) Microbranching instability in phase-field modelling of dynamic brittle fracture. *Appl Phys Lett* 110(15):151903
- Bleyer J, Roux-Langlois C, Molinari JF (2017) Dynamic crack propagation with a variational phase-field model: limiting speed, crack branching and velocity-toughening mechanisms. *Int J Fract* 204(1):79
- Bolander JE, Sukumar N (2005) Irregular lattice model for quasistatic crack propagation. *Phys Rev B* 71(9):094106
- Broberg K (1996) How fast can a crack go? *Mater Sci* 32(1):80
- Camacho GT, Ortiz M (1996) Computational modelling of impact damage in brittle materials. *Int J Solids Struct* 33(20–22):2899
- Červenka J, Bažant ZP, Wierer M (2005) Mechanism-based energy regularization in computational modeling of quasibrittle fracture. *Int J Numer Meth Eng* 62(5):700
- Doan DH, Bui TQ, Van Do T, Duc ND (2017) A rate-dependent hybrid phase field model for dynamic crack propagation. *J Appl Phys* 122(11):115102

- Dugdale DS (1960) Yielding of steel sheets containing slits. *J Mech Phys Solids* 8(2):100
- Ebeida MS, Mitchell SA (2011) Proceedings of the 20th international meshing roundtable. Springer, Berlin, pp 273–290
- F Zhou (1996) Study on the macroscopic behavior and the microscopic process of dynamic crack propagation. Ph.D. thesis, The University of Tokyo, Tokyo
- Fenghua Z, Lili W, Shisheng H et al (1992) Explosion and Shock waves 4
- Fineberg J (1997) APS, pp F4–02
- Fineberg J, Marder M (1999) Instability in dynamic fracture. *Phys Rep* 313(1–2):1
- Freund LB (1998) Dynamic fracture mechanics. Cambridge University Press, Cambridge
- Gorgogianni A, Eliáš J, Le JL (2020) Measurement of characteristic length of nonlocal continuum. *J Appl Mech* 87:9
- Graebing D, Muller R, Paliere J (1993) Linear viscoelastic behavior of some incompatible polymer blends in the melt. Interpretation of data with a model of emulsion of viscoelastic liquids. *Macromolecules* 26(2):320
- Hernández-Jiménez A, Hernández-Santiago J, Macias-García A, Sánchez-González J (2002) Relaxation modulus in PMMA and PTFE fitting by fractional Maxwell model. *Polym Testing* 21(3):325
- Jia JH, Shen XY, Hua HX (2007) Viscoelastic behavior analysis and application of the fractional derivative Maxwell model. *J Vib Control* 13(4):385
- Jirásek M, Bauer M (2012) Numerical aspects of the crack band approach. *Comput Struct* 110:60
- Jirásek M, Grassl P (2008) Evaluation of directional mesh bias in concrete fracture simulations using continuum damage models. *Eng Fract Mech* 75(8):1921
- Jirásek M, Rolshoven S (2003) Comparison of integral-type nonlocal plasticity models for strain-softening materials. *Int J Eng Sci* 41(13–14):1553
- Jo C, Fu J, Naguib HE (2005) Constitutive modeling for mechanical behavior of PMMA microcellular foams. *Polymer* 46(25):11896
- John R, Shah SP (1986) Fracture of concrete subjected to impact loading. *Cem Concret Aggregat* 8(1):24
- Kachanov L (1986) Introduction to continuum damage mechanics, vol 10. Springer, New York
- Kirane K, Su Y, Bažant ZP (2015) Strain-rate-dependent microplane model for high-rate comminution of concrete under impact based on kinetic energy release theory. *Proc R Soc A* 471(2182):20150535
- Knauss W (1970) Delayed failure” the Griffith problem for linearly viscoelastic materials. *Int J FractMech* 6(1):7
- Ladeveze P (1992) A damage computational method for composite structures. *Comput Struct* 44(1–2):79
- Leon S, Spring D, Paulino G (2014) Reduction in mesh bias for dynamic fracture using adaptive splitting of polygonal finite elements. *Int J Numer Meth Eng* 100(8):555
- Li T, Marigo JJ, Guilbaud D, Potapov S (2016) Gradient damage modeling of brittle fracture in an explicit dynamics context. *Int J Numer Meth Eng* 108(11):1381
- Luo W, Chau VT, Bažant ZP (2019) Effect of high-rate dynamic comminution on penetration of projectiles of various velocities and impact angles into concrete. *Int J Fract* 216(2):211
- Mazars J (1986) A description of micro-and macroscale damage of concrete structures. *Eng Fract Mech* 25(5–6):729
- Molinari JF, Gazonas G, Raghupathy R, Rusinek A, Zhou F (2007) The cohesive element approach to dynamic fragmentation: the question of energy convergence. *Int J Numer Meth Eng* 69(3):484
- Needleman A (1988) Material rate dependence and mesh sensitivity in localization problems. *Comput Methods Appl Mech Eng* 67(1):69
- Nguyen VP, Wu JY (2018) Modeling dynamic fracture of solids with a phase-field regularized cohesive zone model. *Comput Methods Appl Mech Eng* 340:1000
- Nguyen H, Pathirage M, Rezaei M, Issa M, Cusatis G, Bažant ZP (2020) New perspective of fracture mechanics inspired by gap test with crack-parallel compression. *Proc Natl Acad Sci* 117:14015–14020
- Pandolfi A, Ortiz M (2002) An efficient adaptive procedure for three-dimensional fragmentation simulations. *Eng Comput* 18(2):148
- Pandolfi A, Krysl P, Ortiz M (1999) Finite element simulation of ring expansion and fragmentation: the capturing of length and time scales through cohesive models of fracture. *Int J Fract* 95(1):279
- Papoulia KD, Sam CH, Vavasis SA (2003) Time continuity in cohesive finite element modeling. *Int J Numer Meth Eng* 58(5):679
- Pereira L, Weerheijm J, Sluys L (2015) In 9th International conference on fracture mechanics of concrete and concrete structures (FraMCoS-9), p 14
- Pontiroli C (1995) Comportement au souffle des structures en béton armé: analyse expérimentale et modélisation. Ph.D. thesis, Cachan, Ecole normale supérieure
- Rabbi MF, Chalivendra VB (2019) Mathematical modeling of viscoelastic material under impact load. *J Strain Anal Eng Design* 54(2):130
- Rabbi M, Chalivendra V, Li D (2019) A novel approach to increase dynamic fracture toughness of additively manufactured polymer. *Exp Mech* 59(6):899
- Ravi-Chandar K, Knauss W (1984) An experimental investigation into dynamic fracture: III. On steady-state crack propagation and crack branching. *Int J Fract* 26(2):141
- Repetto E, Radovitzky R, Ortiz M (2000) Finite element simulation of dynamic fracture and fragmentation of glass rods. *Comput Methods Appl Mech Eng* 183(1–2):3
- Schapery R (1989) On the mechanics of crack closing and bonding in linear viscoelastic media. *Int J Fract* 39(1–3):163
- Scheibert J, Guerra C, Bonamy D, Dalmas D (2012) Understanding fast macroscale fracture from microcrack post mortem patterns, EGUGA, p 10337
- Sharon E, Gross SP, Fineberg J (1995) Local crack branching as a mechanism for instability in dynamic fracture. *Phys Rev Lett* 74(25):5096
- Sharon E, Gross SP, Fineberg J (1996) Energy dissipation in dynamic fracture. *Phys Rev Lett* 76(12):2117
- Simulia (2017) ABAQUS user’s manual, version 2017. Dassault Systemes Simulia Corp., Providence, RI
- Sluys L, De Borst R, Mühlhaus HB (1993) Wave propagation, localization and dispersion in a gradient-dependent medium. *Int J Solids Struct* 30(9):1153
- Wang J, Xu Y, Zhang W (2014) Finite element simulation of PMMA aircraft windshield against bird strike by using a rate and temperature dependent nonlinear viscoelastic constitutive model. *Compos Struct* 108:21

- Williams J (1972) Visco-elastic and thermal effects on crack growth in PMMA. *Int J FractMech* 8(4):393
- Willis J (1967) Crack propagation in viscoelastic media. *J Mech Phys Solids* 15(4):229
- Wolff C, Richart N, Molinari JF (2015) A non-local continuum damage approach to model dynamic crack branching. *Int J Numer Meth Eng* 101(12):933
- Wu JY (2017) A unified phase-field theory for the mechanics of damage and quasi-brittle failure. *J Mech Phys Solids* 103:72
- Wu JY, Nguyen VP (2018) A length scale insensitive phase-field damage model for brittle fracture. *J Mech Phys Solids* 119:20
- Xu XP, Needleman A (1994) Numerical simulations of fast crack growth in brittle solids. *J Mech Phys Solids* 42(9):1397
- Xu D, Liu Z, Liu X, Zeng Q, Zhuang Z (2014) Modeling of dynamic crack branching by enhanced extended finite element method. *Comput Mech* 54(2):489
- Xue J, Kirane K (2019) Strength size effect and post-peak softening in textile composites analyzed by cohesive zone and crack band models. *Eng Fract Mech* 212:106
- Yazid A, Abdelkader N, Abdelmadjid H (2009) A state-of-the-art review of the X-FEM for computational fracture mechanics. *Appl Math Model* 33(12):4269
- Yoffe EH (1951) LXXV. The moving griffith crack. *Lond Edinb Dublin Philosoph Mag J Sci* 42(330):739
- Zhou F, Molinari JF, Shioya T (2005) A rate-dependent cohesive model for simulating dynamic crack propagation in brittle materials. *Eng Fract Mech* 72(9):1383
- Zi G, Chen H, Xu J, Belytschko T (2005) The extended finite element method for dynamic fractures. *Shock Vibrat* 12(1):9

**Publisher's Note** Springer Nature remains neutral with regard to jurisdictional claims in published maps and institutional affiliations.